



Cite this: *New J. Chem.*, 2021, 45, 2453

The influence of triphenylamine as a donor group on Zn–porphyrin for dye sensitized solar cell applications

S. Kotteswaran * and P. Ramasamy

Two donor– π –acceptor type dyes, Zn[10,20-(4-carboxyphenyl)porphyrin] (**Ko-1**) and Zn[5,15-diphenylaminophenyl-10,20-(4-carboxyphenyl)porphyrin] (**Ko-2**), with two different donor units were designed and synthesized for solar cell applications. The **Ko-2** dye contains the triphenylamine group as an electron donor group, the porphyrin unit acts as a π -bridge, and the carboxylic acid group acts as an anchoring group (electron acceptor unit). The **Ko-2** dye has a red-shifted absorption maxima owing to the introduction of the dimethylaminophenyl moiety at the *meso* position of the porphyrin ring. The highly conjugated dimethylaminophenyl group efficiently donates electrons and the electronic interaction between the porphyrin and dimethylaminophenyl unit is better compared to hydrogen. A dye sensitized solar cell (DSSC) was made using commercial P25 TiO₂ material as a photoanode, the Zn–porphyrin derivatives as sensitizers, I⁻/I₃⁻ as an electrolyte, and platinum (Pt) as the counter electrode. The molar extinction coefficient, highest occupied molecular orbital (HOMO), and lowest unoccupied molecular orbital (LUMO) values of the **Ko-2** dye are $1.73 \times 10^5 \text{ M}^{-1} \text{ cm}^{-1}$, -5.82 eV , and -3.35 eV , respectively, which are more suitable for DSSC applications than those of the **Ko-1** dye, which were $1.31 \times 10^5 \text{ M}^{-1} \text{ cm}^{-1}$, -6.16 eV , and -3.60 eV , respectively. The solar cell performance of the **Ko-2**-based DSSC reached 3.3% efficiency with an open circuit voltage (V_{oc}) of 0.68 V, a short circuit photocurrent density (J_{sc}) of 9.69 mA cm^{-2} , and a fill factor (FF) of 0.49; the **Ko-1**-based DSSC reached 1.90% efficiency, a V_{oc} of 0.67 V, a J_{sc} of 5.51 mA cm^{-2} , and a FF of 0.54 under AM 1.5 G irradiation.

Received 20th October 2020,
Accepted 22nd December 2020

DOI: 10.1039/d0nj05060a

rsc.li/njc

1. Introduction

The increasing consumption of fossil fuels, inciting global warming and environmental pollution, has led to a greater focus on renewable energy sources and sustainable development. Increasing energy demand pushes us to find more and more renewable energy sources. Solar energy plays a key role as a renewable, clean and inexhaustible resource and the development of efficient novel molecules to capture and use solar energy more cheaply for solar cell technology is becoming more important. The sensitization of semiconductors with a significant number of dyes for light harvesting has been investigated over the past few years for the development of efficient solar cells.^{1–5} Porphyrin sensitizers were among the first natural types of dyes examined, and to this day they continue to be some of the most frequently studied sensitizers. Recently, the highest efficiency was achieved in the porphyrin sensitized solar cell field when a record efficiency of 13% was reported using a single push–pull porphyrin dye SM315.^{6–8} As many novel types of solar cells have been studied

and developed since the breakthrough by Gratzel and co-workers, the research on dye sensitized solar cells (DSSCs) has intensified in recent years. Recently, the first application of building integrated photo-voltaic technology (BIPV) was demonstrated which showed the potential of a more colorful and transparent solar cell technology.^{9–11} In this type of solar cell, the properties of the dye, such as the color, molecular extinction coefficient and robustness under illumination, are of most importance. However, ruthenium dyes are expensive owing to the cost of ruthenium and the typically lengthy purification steps involved in their preparation. Alternative low cost and readily accessible ruthenium dye replacements are under active investigation. The porphyrins have certain advantages over ruthenium sensitizers. Porphyrin sensitizers can be conveniently synthesized using well-established protocols. Unlike their ruthenium counterparts, these sensitizers are inexpensive, stable and durable. The porphyrin derivatives showed relatively higher molar absorption coefficients; in other words, they are good harvesters. Therefore, considering these advantages and the high efficiency we can say that porphyrins are indeed a good alternative to ruthenium dyes.¹²

The porphyrin based dyes have several advantages, such as a good photostability and rigid molecular structure with large

SSN Research Centre SSN College of Engineering, Kalavakkam, Chennai-603110, India. E-mail: kotties555@gmail.com

absorption coefficients in the visible region. In addition, four *meso* and eight beta positions of porphyrins are available for functionalization which lead to fine tuning of their optical, physical and electrochemical properties and make them more feasible for use in DSSCs.^{13,14} Nature accomplishes increased light absorption by stacking of the chlorophyll-containing thylakoid membranes of the chloroplast to form a disc shaped structure that acts as a light harvesting antenna. This structure absorbs the incident light and then directs the excitation energy to the reaction centers, where light-induced charge separation takes place.^{15,16} Based on their primary role in photosynthesis, the use of porphyrins as light harvesters on semiconductors is particularly attractive. Owing to the delocalized macrocyclic structure and the strong, more intense absorption in the 400–450 nm region (Soret band) as well as the less intense absorption bands (2–4 times) in the 500–700 nm region (Q-bands), porphyrins have been studied extensively and proved to be promising components for molecular electronic and photonic devices.^{17,18} A great number of artificial photonic assemblies based on multi-porphyrin architectures have been designed to mimic photosynthetic solar energy transduction by converting the excitation energy to the chemical potential in the form of long-lived charge separation.¹⁹ Recently, Kim *et al.* reported the photovoltaic activities of various beta-functionalized porphyrin dyes.²⁰ This work was motivated by the consideration that the functionalization of porphyrins at the pyrrolic beta-position with p-conjugative linkers could represent a possible strategy for the preparation of more efficient DSSCs. The resulting extension of the p-conjugation framework, along with the anchoring group (*e.g.*, carboxylic acid) allows a more effective injection of electrons into the conduction band of the semiconductor, which acts as a photoanode. On this basis, the use of a porphyrin containing both the conjugated anchoring carboxyl groups and a donor group attached at a *meso* position was expected to give rise to highly effective DSSCs. Therefore, the rational design of efficient porphyrin dyes, having good light harvesting abilities in the visible and near IR regions is important to obtain a large photocurrent response. Appropriate donor-acceptor groups on the porphyrin ring can significantly broaden

the Soret band, as well as the Q bands, which leads to their enhanced light absorbing properties, as well as the photovoltaic efficiency.

Herein, we have designed and synthesized two Zn-porphyrin dyes, Zn[10,20-(4-carboxyphenyl)porphyrin] (**Ko-1**) and Zn[5,15-diphenylaminophenyl-10,20-(4-carboxyphenyl)porphyrin] (**Ko-2**). The structures of the synthesized dyes were characterized using NMR spectroscopy. The dye sensitized solar cell (DSSC) was made using commercial TiO₂ material as a photoanode, Zn-porphyrin derivatives as a sensitizer, I⁻/I₃⁻ as an electrolyte and platinum (Pt) as a counter electrode. The highest power conversion efficiency of the two Zn-porphyrin derivatives was achieved using the **Ko-2** based on DSSC and reached 3.35%, the **Ko-1** based DSSC reached 1.90%. The optical, electrochemical, time-dependent density-functional theory (TD-DFT) and photovoltaic performance of these dyes have been analyzed and discussed.

2. Experimental section

2.1 Materials and reagents

All of the starting materials were purchased from Sigma Aldrich and Merck. Methyl 4-formylbenzoate, pyrrole, InCl₃, formaldehyde, *p*-chloranil, Et₃N, Zn (OAc)₂ · 2H₂O, KOH, HCl, diphenylaminobenzaldehyde, trifluoroacetic acid (TFA), methanol, hexane, chloroform, methylformamide were obtained, and all chemicals and solvents used in this work were of analytical grade and were used without further purification. All chromatographic separations were carried out on silica gel (120–160 mesh).

2.2 Formation of the porphyrin ring

4-Formylbenzoic acid (2 mmol) and pyrrole (2 mmol) with DDQ were stirred for 2 h at room temperature, 250 ml of chloroform was added and argon gas was passed over for 40 min. Formaldehyde (2 mmol) and trifluoroacetic acid (2 mmol) were added and the obtained solution was stirred in the dark under a nitrogen atmosphere for 15 h. Finally, the *p*-chloranil (6 mmol) was added and the solution was stirred for 3 h. Triethylnitride (2 ml) was added to complete the reaction. The solvent was

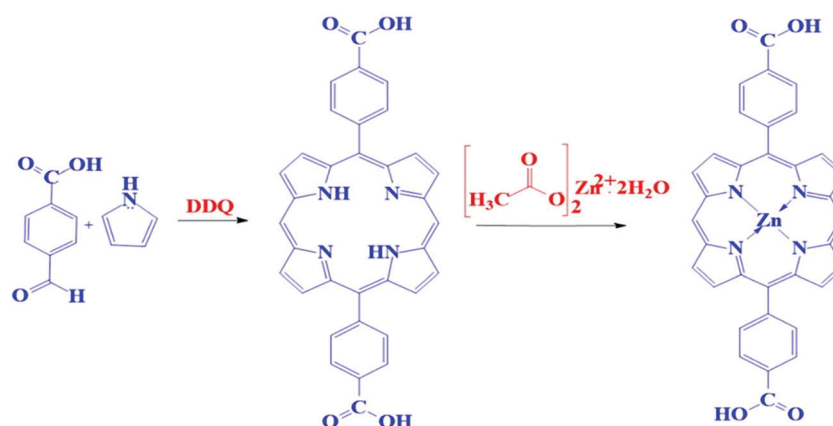


Fig. 1 The Zn-porphyrin reaction scheme.

evaporated and the mixture was passed through thin layer chromatography (TLC) silica to remove the non-porphyrin products and then purification was performed using column chromatography using chloroform : hexane (95 : 5) as an eluent to give the porphyrin as a pure product (2.2). ^1H NMR (400 MHz, DMSO-d_6) δ (ppm): 11.3 (s, 2H, COOH), 8.3 (s, 4H, porphyrin pyrrolic H), 8.09 (s, 4H, porphyrin pyrrolic H), 8.06 (d, $J = 12$ Hz, 4H, aromatic H), 7.29 (d, $J = 12$ Hz, 4H, aromatic H), 4.95 (s, 2H, porphyrin H), 1.25 (s, 2H, porphyrin NH). ^{13}C NMR (400 MHz, DMSO-d_6) δ (ppm) 190.4, 153.4, 148, 146.3, 131.4, 129.8, 129, 126.4, 125.2, 124.5, 123.7, 122.4, 119.5, 77.8, 76.8.

2.3 Metallization of Zn-porphyrin (Ko-1)

A solution of 2.2 (2 mmol) in 15 ml of CHCl_3 and the methanol solution of zinc acetate dehydrate (1.5 mmol) were combined together and the solution was refluxed under a nitrogen atmosphere for 6 h. The solvent was evaporated and the residue was washed with distilled water (20 ml). Then, the solvent was evaporated and the resulting residue was added to 10 ml of distilled water and then dried under vacuum to give the final product **Ko-1**, the reaction scheme for the Zn-porphyrins is shown in Fig. 1. ^1H NMR (400 MHz, DMSO-d_6) δ (ppm): 9.79 (s, 2H, COOH), 7.86 (s, 4H, porphyrin pyrrolic H), 7.67 (s, 4H, porphyrin pyrrolic H), 7.33 (d, $J = 8$ Hz, 4H, aromatic H), 7.31 (d, $J = 6.4$ Hz, 4H, aromatic H), 1.69 (s, 2H, porphyrin-H). ^{13}C NMR (400 MHz, DMSO-d_6) δ (ppm) 167, 134, 130.2, 129.8, 129.4, 128.9, 128.4, 119.7, 117.8, 117.2, 108.8, 108.4, 107, 77.9, 5.57.

2.4 Formation of the porphyrin ring

4-Formylbenzoic acid (2 mmol), pyrrole (2 mmol) and DDQ (2 mmol) were stirred for 2 h at room temperature in 250 ml of chloroform under argon gas for 40 min. Diphenylaminobenzaldehyde (2 mmol) and trifluoroacetic acid (2 mmol) were added and the obtained solution was stirred in the dark under a nitrogen atmosphere for 18 h. Finally, the *para*-chloranil

(6 mmol) was added and the resulting mixture was stirred for 3 h.

Triethylnitrate (2 ml) was added to complete the reaction. The solvent was evaporated and the mixture was passed through TLC silica to remove the impurities and then purification was performed by column chromatography using dichloromethane : ethyl acetate (95 : 5) as an eluent to give porphyrin as a pure product (2.4). ^1H NMR (400 MHz, DMSO-d_6) δ (ppm): 9.1 (s, 2H, COOH), 8.82 (s, 2H, porphyrin pyrrolic H), 8.78 (s, 2H, porphyrin pyrrolic H), 8.75 (s, 2H, porphyrin pyrrolic H), 8.24 (s, 4H, porphyrin pyrrolic H), 8.18 (s, 2H, porphyrin NH), 7.91 (d, $J = 8.4$ Hz, 4H, aromatic H), 7.88 (d, $J = 8.4$ Hz, 4H, aromatic H), 7.24 (d, $J = 5.6$ Hz, 4H, aromatic H), 7.22 (d, $J = 5.6$ Hz, 4H, aromatic H), 7.18 (d, $J = 8.8$ Hz, 6H, aromatic H), 6.67 (d, $J = 2.8$ Hz, 6H, aromatic H), 6.64 (d, $J = 2.4$ Hz, 6H, aromatic H). ^{13}C NMR (400 MHz, DMSO-d_6) δ (ppm) 174.8, 164.7, 163.8, 163.1, 161, 160.8, 157.8, 157.2, 156.7, 156.3, 156, 149, 146, 135.2, 116.3, 112.3, 60.5, 58.07, 56.7, 46.01.

2.5 Metallization of Zn-porphyrin (Ko-2)

The solution of 2.4 (1 mmol) in 15 ml of CHCl_3 and methanol solution of zinc acetate dehydrate (1.5 mmol) were added and the solution was refluxed under a nitrogen atmosphere for 8 h. The solvent was evaporated, the residue was washed with distilled water (20 ml) and then dried under vacuum to give the final purple product of **Ko-2**. The reaction mechanism for the synthesized dyes is shown in Fig. 2. ^1H NMR (400 MHz, DMSO-d_6) δ (ppm): 11.6 (s, 2H, COOH), 9.68 (s, 2H, porphyrin pyrrolic H), 9.46 (s, 2H, porphyrin pyrrolic H), 9.32 (s, 2H, porphyrin pyrrolic H), 9.25 (s, 4H, porphyrin pyrrolic H), 7.86 (d, $J = 12$ Hz, 4H, aromatic H), 7.72 (d, $J = 12$ Hz, 4H, aromatic H), 7.58 (d, $J = 9.2$ Hz, 4H, aromatic H), 7.43 (d, $J = 9.2$ Hz, 4H, aromatic H), 7.40 (d, $J = 8.4$ Hz, 6H, aromatic H), 7.38 (d, $J = 8.4$ Hz, 6H, aromatic H), 7.06 (d, $J = 8$ Hz, 6H, aromatic H). ^{13}C NMR (400 MHz, DMSO-d_6) δ (ppm) 178.4, 172.4, 167.3, 156.5,

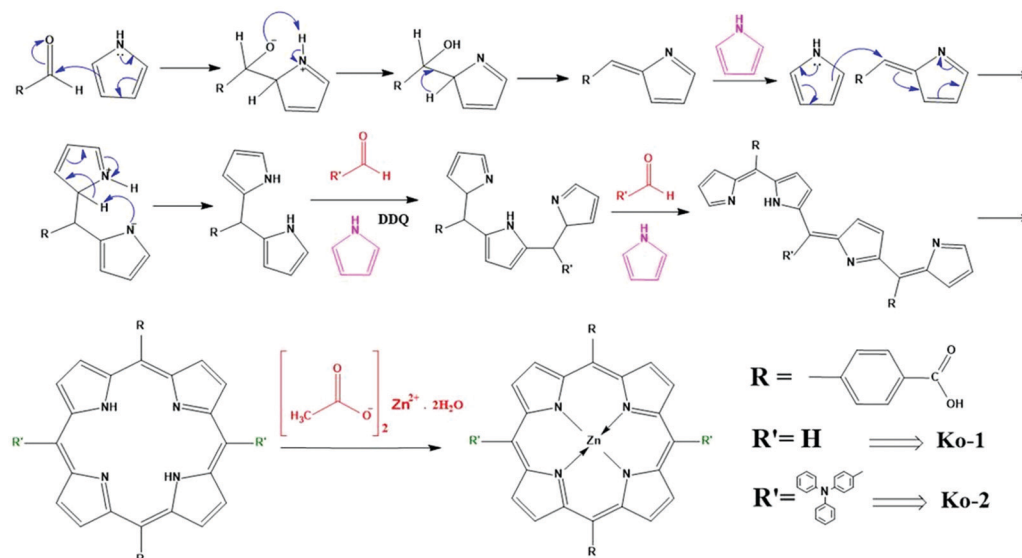


Fig. 2 The reaction mechanism for the **Ko-1** and **Ko-2** dyes.

156.2, 148.2, 148, 147.6, 147.4, 147.1, 145.1, 143.8, 143.2, 142.7, 142.3, 140.6, 140, 138.2, 132.8, 131.8, 48.5.

3. Solar cell fabrication

Fluorine doped SnO₂ glass (FTO 7 Ω cm⁻²) was washed with isopropanol, ethanol and deionized water using an ultrasonic bath for 30 min. The TiO₂ nanoparticles (Degussa P25 Solaronix) were ground for an appropriate time using Triton-X 100, acetyl acetone, ethanol and water to make a colloid blend. A 10 μm thick film of TiO₂ nanoparticles was deposited onto the side of the conducting layer of fluorine-doped tin oxide (FTO) glass using the doctor blade technique. TiO₂ substrates were sintered at 450 °C for 30 minutes in air. The FTO glass (15 Ω cm⁻²) was washed with isopropanol, ethanol and deionized water using an ultrasonic bath for 30 min. The FTO glass was treated with 40 mM TiCl₄ aqueous solution at 70 °C for 40 min and then the substrates were sintered at 430 °C for 30 min.

After cooling to 80 °C the TiO₂ electrodes were immersed in the 0.5 mM dye solutions in dimethylformamide and left for 24 h at room temperature. After dye adsorption, the dye coated TiO₂ electrodes were cleaned. Pt (Platisol Solaronix) was deposited onto the side of the conducting layer of another FTO using doctor blading as the counter electrode and then the substrates were sintered at 450 °C for 30 min in air. The photovoltaic measurements were performed in a sandwich cell consisting of the porphyrin dyes sensitized TiO₂ electrode as the working electrode and Pt as the counter electrode. The electrolyte consists of a I⁻/I₃⁻ (Iodolyte Solaronix) redox potential and the efficient irradiated area of the cell was 0.5 × 0.5 cm. The photocurrent–voltage (*J*-*V*) characteristics were measured using an Oriel Class-AAA Simulator (Newport) with a xenon lamp as a light source having an intensity of 100 mW cm⁻². Prior to the experiment the light intensity was adjusted with a standard PV reference cell (2 × 2 cm monocrystalline silicon solar cell, calibrated at NREL, Colorado, USA) with a Keithley 2400 source-measure unit.

All photovoltaic properties such as the open circuit voltage (*V*_{oc}), short circuit current density (*J*_{sc}), and fill factor (FF) were obtained from the *J*-*V* curve and used in the following equation to obtain the power conversion efficiency.

$$\text{Efficiency} = \frac{J_{sc} (\text{mA cm}^{-2}) \times V_{oc} (\text{V}) \times \text{FF}}{P_{in} (\text{mW cm}^{-2})}$$

4. Characterization techniques

The ¹H NMR and ¹³C NMR spectra of all the synthesized compounds were recorded in DMSO-d₆ on a Bruker AV III 500 MHz FT NMR spectrometer. The UV-Vis absorption spectra of the dyes in different solvents and the diffuse reflectance spectra were recorded on a PerkinElmer Lambda 35 UV-Vis NIR spectrophotometer. The mass spectrometry of all the synthesized compounds were recorded on a gas chromatography (GC)-mass spectrometer. Cyclic voltametric studies were carried out with a ZAHNER IM66 Electrochemical Analyzer using glassy-carbon as

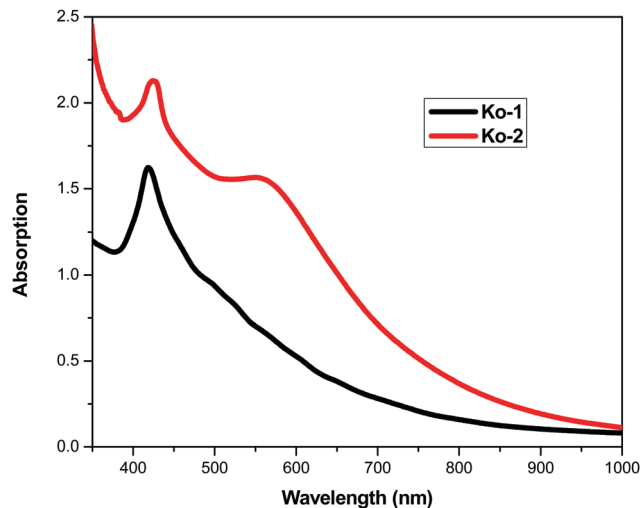


Fig. 3 Absorption spectra of the Ko-1 and Ko-2 dyes.

the working electrode, platinum as the counter electrode and Ag/AgCl as the reference electrode. The redox potential of the dye was measured in DMF with 0.1 M TBAPF₆ with a scan rate of 100 mV s⁻¹.

The photovoltaic performance of the DSSC was evaluated using a Xenon lamp with a light intensity of 100 mW cm⁻² and integrated to an air mass (AM) 1.5 G filter (Sciencetech, Canada). The *J*-*V* curves were measured using a Keithley Model 2400 multisource meter. Prior to the experiment the light intensity was adjusted with a standard photovoltaic (PV) reference cell (2 × 2 cm monocrystalline silicon solar cell, calibrated at NREL, Colorado, USA). All of the photovoltaic properties, such as the *V*_{oc}, *J*_{sc}, FF and power conversion efficiency (PCE) (*η*) efficiency were derived from the *J*-*V* curves. The active area of the cell was 5 × 5 mm.

5. Results and discussion

5.1 UV-Vis NIR absorption analysis

The UV-Vis absorption spectra of Ko-1 and Ko-2 in DMF solution are shown in Fig. 3 and the peak positions and molar absorption coefficients of the Soret and Q-bands of the porphyrin dyes are listed in Table 1. The UV-Vis absorption spectrum of Ko-1 exhibits a strong Soret band at 421 nm. However, Ko-2 showed strong and moderate absorption peaks at 425 and 564 nm, respectively. The strong intense Soret band for the Ko-1 and Ko-2 dyes between 380 to 480 nm is due to the intramolecular π-π* electronic transition and the porphyrin species consist of a strong transition to the second excited state (S₀-S₂). The broad, less intense second Q-band of the Ko-2 dye

Table 1 Absorption data for the Ko-1 and Ko-2 dyes

Dye	Absorption maximum (nm)	Molar extinction coefficient (ε/10 ⁵ M ⁻¹ cm ⁻¹)
Ko-1	421	1.312
Ko-2	425, 564	1.73, 1.25

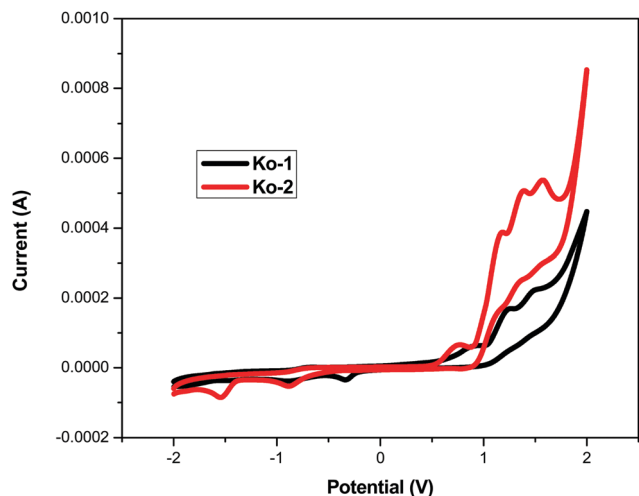


Fig. 4 Cyclic voltammety data from **Ko-1** and **Ko-2**.

between 580 to 650 nm is due the intramolecular $n-\pi^*$ electronic transition and this involves a weak transition to the first excited state (S_0-S_1).

As seen on the UV-Vis absorption spectrum, the Soret band of **Ko-2** at 425 nm is 4 nm red-shifted compared with those of compound **Ko-1** (421 nm).

In addition, the **Ko-2** dye contains the Q-band at 564 nm. The **Ko-2** dye has a long region of absorption. This is because the **Ko-2** dye contains triphenylamine in the *meso*-position which has more conjugated double bands and also has an electron withdrawing nature compared to the **Ko-1** dye, which is able to absorb the higher energy from the electromagnetic spectrum. The molar extinction coefficient (ϵ) of the **Ko-1** Soret band is $1.31 \times 10^5 \text{ mol L}^{-1} \text{ cm}^{-1}$ and the **Ko-2** dye Soret band is $1.73 \times 10^5 \text{ mol L}^{-1} \text{ cm}^{-1}$, which is higher than that of **Ko-1**. As a consequence of the extended π -conjugation, the molar extinction coefficient of **Ko-2** is significantly higher than that of **Ko-1**. The molar extinction coefficient of the **Ko-2** Q-band is $1.25 \times 10^5 \text{ mol L}^{-1} \text{ cm}^{-1}$. This is because of the electronic interaction between the triphenylamine with the porphyrin group. This type of electronic interaction is not available in **Ko-1**. These results indicate that **Ko-1** has a relatively weak light harvesting ability compared to **Ko-2**. From the above results we can conclude that the triphenylamine moiety has more phenyl-conjugated double bonds and therefore a greater light harvesting capability (Xiang *et al.* 2011).

5.2. Electrochemical analysis

Electrochemical studies were performed on the four dyes to elucidate the effect of the thienyl groups on the energy level of

the porphyrin macro-cycle. The reduction potentials were measured using differential pulse voltammetry (DPV) and the oxidation potentials (E_{ox}) corresponding to the HOMO (highest occupied molecular orbital) energy levels of the porphyrin dyes were determined *via* cyclic voltammetry, as shown in Fig. 4. The E_{ox} is the first oxidation potential (*vs.* NHE), and E_0e_0 is determined from the intercept of the normalized absorption and emission spectra. We then considered the potential levels of ($E_{\text{ox}} - E_{\text{red}}$) corresponding to the LUMO (lowest unoccupied molecular orbital) level of the dyes. By the introduction of thienyl groups at the *meso*-positions of the porphyrin dyes, the energy level of LUMO is significantly shifted to the positive compared with the reference PZn²¹ and the HOMO energy levels are negatively shifted, indicating a decreased HOMO–LUMO energy gap. Furthermore, for dyes **Ko-1** and **Ko-2** with the introduction of electron donating groups into the porphyrin ring, a decrease of the HOMO–LUMO energy gaps relative to PZn is observed, which is consistent with the red-shift in the absorption and emission spectra. As shown in Table 2, the sufficiently low HOMO energy level of the dye will ensure that there is sufficient driving force for the dye regeneration reaction to efficiently compete with the recapture of the injected electrons using the dye cation radical. Although the LUMO energy level is more negative than the conduction band (CB) of TiO₂ (-0.5 V vs. NHE),^{22–28} indicating a sufficient driving force for electron transfer from the excited dye molecules to the conduction band of the TiO₂ electrode.

Electrochemical studies were performed on the two dyes to elucidate the effect of the triphenylamine group on the energy level of the porphyrin macro-cycle. The E_{ox} corresponding to the HOMO energy levels of the porphyrin dyes were determined *via* cyclic voltammetry. The cyclic voltammetry measurements for **Ko-1** and **Ko-2** in DMF were analyzed using TBAPF₆ (0.1 M) as the supporting electrolyte at a scan rate of 100 mV s^{-1} using a three electrode system. All of the potentials are quoted with respect to non-aqueous silver/silver chloride as a reference electrode, this electrode was externally calibrated with the Fe/Fe⁺ redox couple in dimethylformamide solution and has a potential of $0.558 \text{ V versus NHE}$ and was calibrated with ferrocene. E_{ox} is the first oxidation potential (*vs.* NHE) and E_{0-0} is determined from the intercept of the normalized absorption spectra. We then considered the potential levels of ($E_{\text{ox}} - E_{0-0}$) corresponding to the LUMO level of the dyes.^{29–32}

The anodic and cathodic potentials of **Ko-1** are 1.22, -0.33 and 1.51, -0.90 respectively. The anodic and cathodic potentials of **Ko-2** are 1.17, -0.90 and 1.58, -1.56 respectively. The HOMO value of the **Ko-1** is 6.61 eV and the LUMO value is -3.60 eV. The HOMO value of the **Ko-2** is 5.82 eV and the LUMO value is -3.35 eV. By introducing the triphenylamine

Table 2 Electrochemical and simulation results for the **Ko-1** and **Ko-2** dyes

Dye	Oxidation (V)	Reduction (V)	HOMO (eV)		LUMO (eV)		Band gap (eV)	
			Exp.	Theory	Exp.	Theory	Exp.	Theory
Ko-1	1.22, 1.51	-0.33 , -0.90	-6.16	-6.34	-3.60	-3.45	2.56	2.89
Ko-2	1.17, 1.58	-0.90 , -1.56	-5.82	-5.94	-3.35	-3.25	2.46	2.69

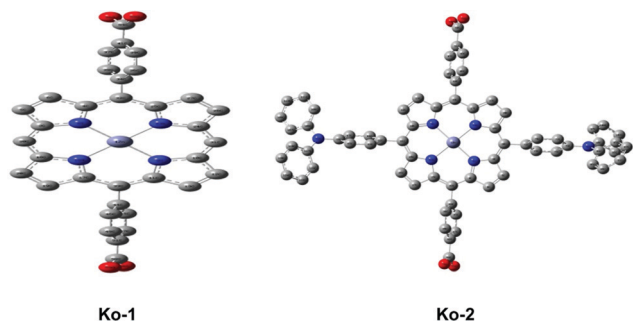


Fig. 5 Optimized molecular structures of **Ko-1** and **Ko-2** (hydrogen atoms are omitted for clarity).

group in the **Ko-2** dye at the *meso*-position the energy level of the LUMO is significantly shifted to the positive side compared to the **Ko-1** dye (Xiang *et al.* 2011) and the HOMO energy level is negatively shifted, indicating a decreased HOMO–LUMO energy gap. Furthermore, upon the introduction of TPA into the porphyrin ring, a decrease in the HOMO–LUMO energy gaps relative to **Ko-2** is observed, which is consistent with the red-shift in the absorption spectrum. The sufficiently low HOMO

energy level of the dye will ensure that there is enough driving force for the dye regeneration reaction to compete efficiently with the recapture of the injected electrons by the dye cation radical. Although the LUMO energy level is more negative than the CB of TiO₂ (Zhou *et al.* 2011), indicating sufficient driving force for the electron transfer from the excited dye molecules to the CB of the TiO₂ electrode. The HOMO value of the **Ko-2** dye is -5.82 eV which is lower than the redox potential of the I[−]/I₃[−] value (-4.94 eV) and the LUMO value is -3.35 eV, which is higher than the CB value of TiO₂ (-4.04 eV). These results indicate that the **Ko-2** dye can easily inject the electron into the semiconductor and can easily gain electrons from the redox couple, therefore the **Ko-2** dye is more suitable for DSSC applications compared to the **Ko-1** dye.

5.3 Computational details

All calculations were performed using the Gaussian 09 W program. The B3LYP density functional with the 6-311G(d,p) basis set was used for geometric optimization. The electronic excitations were studied using TD-DFT. TD-DFT calculations were performed using CAM-B3LYP with the 6-311G(d,p) basis set.

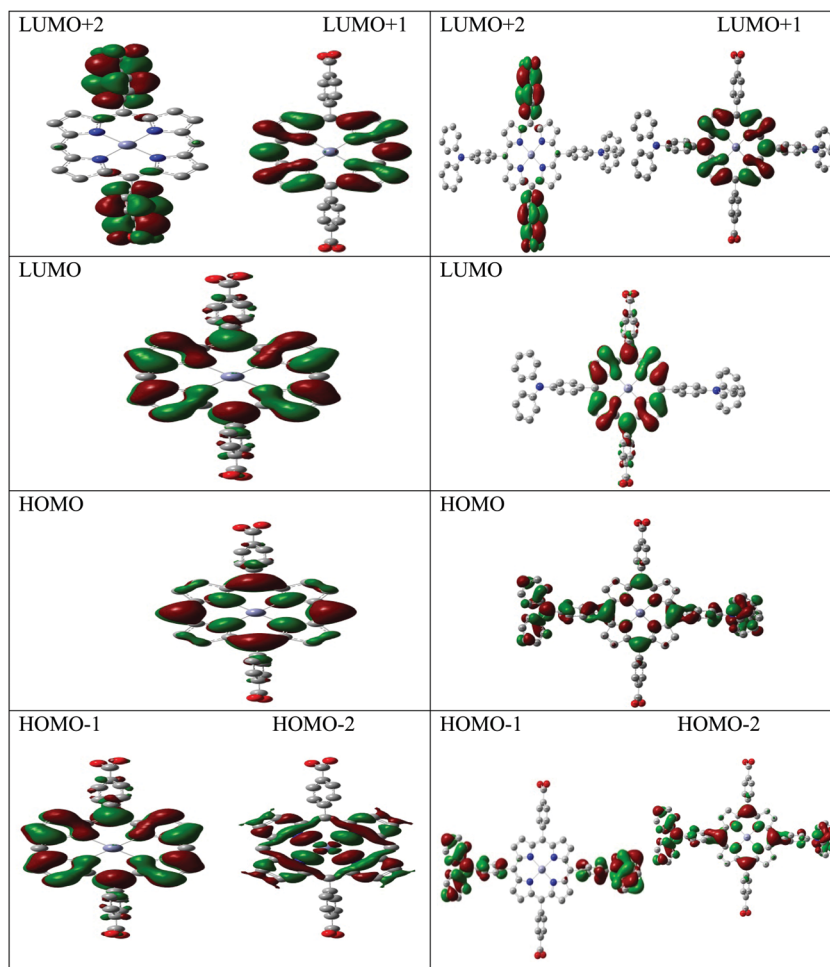


Fig. 6 Frontier molecular orbitals of **Ko-1** (left) and **Ko-2** (right).

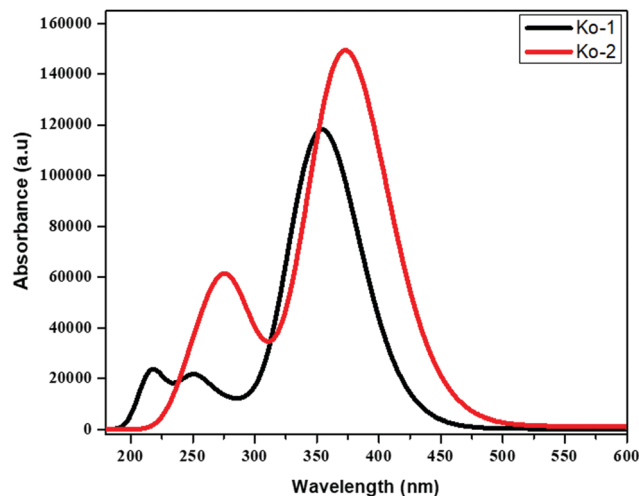


Fig. 7 Simulated absorption spectra of **Ko-1** and **Ko-2**.

The optimized molecular structure of **Ko-1** and **Ko-2** are presented in Fig. 5. The hydrogen atoms are omitted in the optimized structure and also the frontier molecular orbitals for clarity. HOMO-2, HOMO-1, HOMO, LUMO, LUMO+1 and LUMO+2 for dyes **Ko-1** and **Ko-2** are shown in Fig. 6. The HOMO is mainly present in the central core of the porphyrin core for **Ko-1** and **Ko-2**. The HOMO is mainly contributed by the central core and triphenylamine part of the dye sensitizers. The LUMO of the dye is mainly presented in the central core of the dye sensitizers. The HOMO energies are different owing to the triphenylamine part in **Ko-2**. The **Ko-2** results show the reduced energy gap of the sensitizer. This is due to the donating ability of triphenylamine. The HOMO-LUMO energy gaps for **Ko-1** and **Ko-2** in the gas phase are 2.89 and 2.69 eV, respectively. The charge separated state is one of the factors that influences the solar cell efficiency. The HOMO energy levels and HOMO-LUMO energy gaps help to predict the efficiency of the solar cells.³³⁻⁴⁰

The simulated electronic absorption spectrum for **Ko-1** and **Ko-2** dye is depicted in Fig. 7. The corresponding molecular orbital transitions are presented in Table 3. The maximum wavelength was a result of the HOMO → LUMO (53%) for **Ko-1** and the HOMO-1 → L+1 (43%) for **Ko-2**. The wavelength maximum were 545 and 561 nm for **Ko-1** and **Ko-2** respectively. From the spectra it can be seen that **Ko-2** was red shifted compared to **Ko-1**. The red shift in the **Ko-2** dye was due to the introduction of the triphenylamine group in the meta position. The reduced energy gap and maximum absorption wavelength

Table 3 Electronic transition characteristics of the **Ko-1** and **Ko-2** dyes

Dye	Energy (eV)	Wavelength (nm)	Oscillator strength	Major electronic contribution
Ko-1	2.28	545	0.0045	H → L (53%)
	3.49	356	2.0119	H → L (46%)
	3.54	351	0.9131	H → L+1 (50%)
Ko-2	2.22	561	0.0141	H-1 → L+1 (43%)
	2.22	560	0.0153	H-1 → L (45%)
	3.29	377	2.1521	H-1 → L (47%)

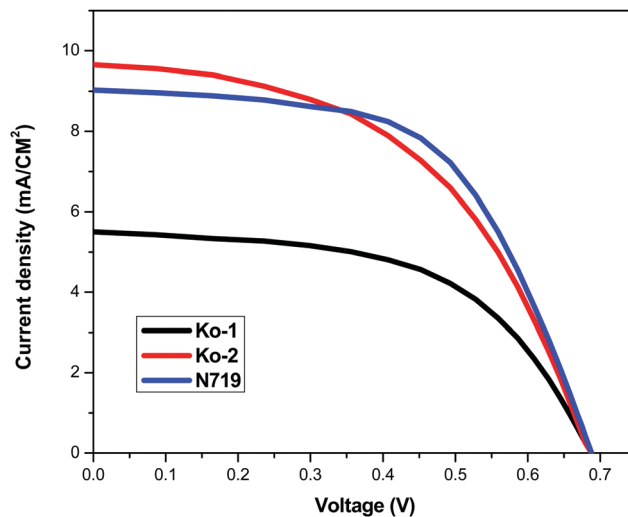


Fig. 8 *J*-*V* curves under the illumination of simulated solar AM 1.5G irradiation.

was reflected in the efficiency. The **Ko-2** dye shows a higher photo conversion efficiency than the **Ko-1** dye.³³⁻³⁹

5.4 Photovoltaic performance of the DSSC

In order to study the influence of the donor units of **Ko-1** and **Ko-2** on the DSSC device performance, photovoltaic experiments were conducted. The devices were assembled using a layer of TiO₂ in conjugation with an iodide-triiodide based electrolyte, as described above. Fig. 8 shows the *J*-*V* characteristics of the DSSC devices sensitized by **Ko-1** and **Ko-2** under a standard air mass 1.5 global spectral solar photon flux (AM 1.5 G with a light intensity of 100 W cm⁻²). The *J*_{sc}, *V*_{oc} and FF of the two devices are summarized in Table 4. Although the spectral response of the DSSC devices stained with dyes **Ko-1** and **Ko-2** appeared to be 1.90% and 3.35%, respectively. This implies the enhancement of the photo-induced charge collection of the **Ko-2** dye based devices over **Ko-1** dye based devices. It can be concluded from these preliminary results that the DSSCs sensitized with **Ko-2** bearing the electron donating triarylamine core unit, achieved a better photovoltaic performance than those sensitized with the **Ko-1** hydrogen unit.

Table 4 *J*-*V* characteristics of the **Ko-1** and **Ko-2** sensitizers and an N719 sensitized solar cell with a liquid electrolyte under AM 1.5 irradiation conditions

S. no.	Dyes	<i>J</i> _{sc} (mA cm ⁻²)	<i>V</i> _{oc} (V)	FF	Efficiency (η, %)
1	Ko-1	5.51	0.62	0.54	1.90
		6.3	0.71	0.43	1.97
		6.30	0.71	0.41	1.87
2	Ko-2	9.69	0.68	0.49	3.30
		8.63	0.76	0.51	3.35
		8.59	0.76	0.49	3.25
3	N719	9.0	0.67	0.57	3.45
		8.49	0.75	0.53	3.38
		8.70	0.76	0.51	3.42

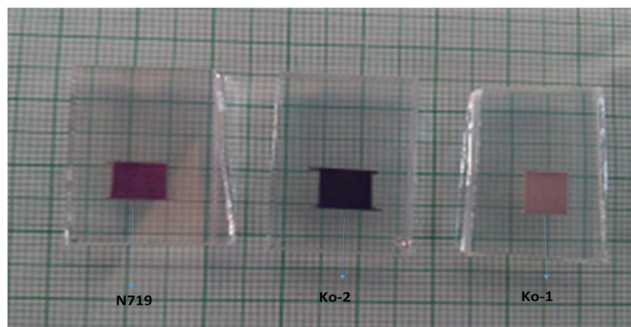


Fig. 9 Photoanodes made of the three kinds of dyes (commercially available N719 dye, **Ko-1** and **Ko-2** dyes).

Moreover, the lower PCE of the **Ko-1** dye based DSSCs compared with that of the **Ko-2** dye based DSSCs was mainly caused by a low J_{sc} that is attributed to the excessive electro-negativity of the core unit, possibly reducing the efficiency of the electron injection from the **Ko-1** molecules to TiO_2 . The dye **Ko-2** gave the best performance. The conversion efficiency was 3.35% with a J_{sc} of 9.69 mA cm^{-2} , V_{oc} of 0.68 V and FF of 0.49. Dye **Ko-1** gave a conversion efficiency of 1.90% with J_{sc} 5.51 mA cm^{-2} , V_{oc} 0.67 V and FF 0.54. The **Ko-1** and **Ko-2** dye based solar cell devices were fabricated under similar conditions.

The highest J_{sc} of **Ko-2** compared with other devices in this study is attributed to the high extinction coefficient. As we know, the aggregation of the dye could decrease the V_{oc} , the triphenylamine moiety, as a donating group, could effectively suppress the dye-aggregation (Sato *et al.* 2003; Sato *et al.* 2005). Otherwise, the increase in the intramolecular charge separation may benefit from the increase of the V_{oc} (Ooyama *et al.* 2009). Accordingly, the dye **Ko-2** gave the best performance, the conversion efficiency was 3.35% with a J_{sc} of 9.69 mA cm^{-2} , V_{oc} of 0.68 V and FF of 0.49, giving the largest V_{oc} . Therefore, the performance of these dyes has improved owing to the increase in the photocurrent and open circuit voltage. We believe that the intramolecular charge separation and broad absorption bands

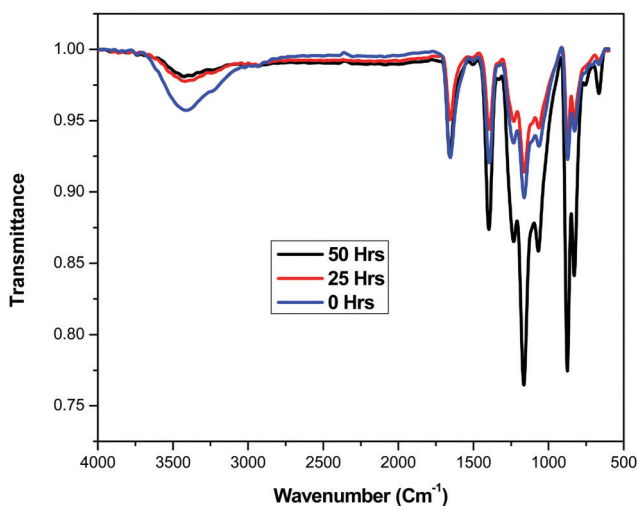


Fig. 10 FTIR spectra of the **Ko-1** dye irradiated by sunlight after 0, 25 and 50 h.

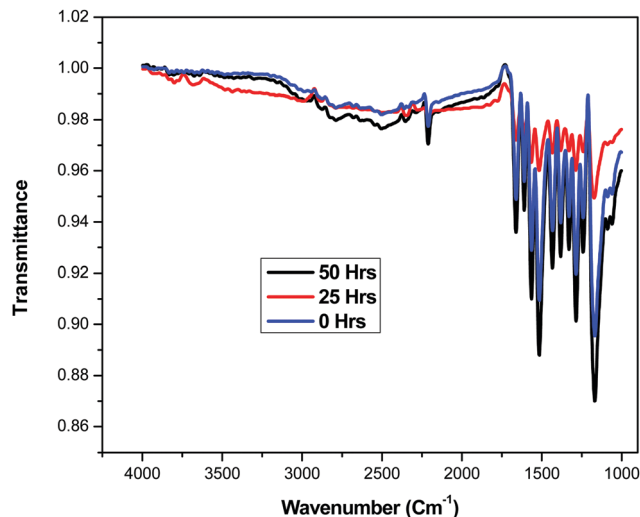


Fig. 11 FTIR spectra of the **Ko-2** dye irradiated by sunlight after 0, 25 and 50 h.

with a high extinction coefficient are responsible for the significant enhancement of the conversion efficiency.

5.5 Dye adsorption measurements

To determine the amount of dye molecules adsorbed on the TiO_2 surface we prepared 0.5 mM of **Ko-1** and **Ko-2** dye solutions, then analyzed these using the UV-Vis NIR spectrum. Using these absorption values the molar extinction coefficient of the initial dye solutions was calculated through the Beer-Lambert law. TiO_2 films were immersed in the same dye solutions for 24 h, after that the TiO_2 films were taken out. Dye desorption was carried out using 0.5 mM of NaOH in a mixed solvent (water: DMF = 1:9, v/v). Then, the UV-Vis absorption spectra of the resultant solutions were measured to estimate the amount of adsorbed dye molecules. The amount of **Ko-1** and **Ko-2** dye molecules adsorbed onto the TiO_2 surface were $1.3 \times 10^{-8} \text{ M cm}^{-2}$ and $0.9 \times 10^{-8} \text{ M cm}^{-2}$. The **Ko-2** based device gave a high dye

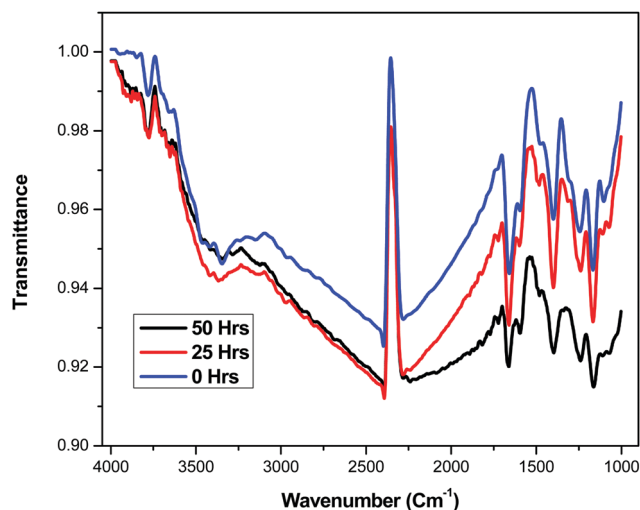


Fig. 12 FTIR spectra of the N719 dye irradiated by sunlight after 0, 25 and 50 h.

adsorption, therefore the **Ko-2** based DSSC gave a higher current (J_{sc}) which leads to a higher solar cell performance.

5.6 Photostability

The stability of the three kinds of dyes were analyzed using sunlight irradiated onto the photoanode, as shown in Fig. 9.

After 0, 25, and 50 h the Fourier transform infrared spectroscopy (FTIR) spectrum of the dye molecules was analyzed and the spectrum is shown in Fig. 10 for **Ko-1**, Fig. 11 for **Ko-2** and Fig. 12 for the N719 dye, respectively. The sunlight irradiated **Ko-1** dye based photoanode FTIR spectrum remained stable for up to 25 h, after that the degradation started and continued up to 50 h. The **Ko-2** based photoanode was stable up to 50 h because its FTIR spectrum remained similar up to 50 h. The N719 dye was not stable because its FTIR spectrum did not remain similar up to 50 h. Therefore, the present **Ko-2** dye molecule revealed a very good photostability and the dye molecule is suitable for stable DSSC applications.

6. Conclusions

Two Zn-porphyrin dyes, **Ko-1** and **Ko-2**, have been synthesized and applied in DSSCs. As a consequence of extended p-conjugation, both the Soret and Q bands of **Ko-2** exhibit significant red shifts and a Soret band broader than that of **Ko-1** is seen, because the electronic interaction with the porphyrins is more pronounced for triphenylamine than for hydrogen. The results clearly show that p-conjugation, with a highly conjugated arylamine unit, can improve the light-harvesting capabilities of porphyrin dyes; **Ko-2** exhibits a greater power conversion efficiency of 3.35%. Further structural modification of the *meso*-substituted porphyrins and increasing the conjugated double bonds in their structure may improve the performance of the solar cells. Furthermore, their easy synthesis, low cost, and easy availability make these Zn-porphyrin-based dyes promising sensitizer materials that are suitable for the development of industrial DSSCs in the near future.

Conflicts of interest

There are no conflicts to declare.

Acknowledgements

The authors thank SIF, VIT, Vellore for NMR analysis; SAIF, IIT, Madras for providing mass spectrometry analysis; and CSIR (08/542(0008)/19 EMR-1) for financial support.

References

- B. Oregan and M. Gratzel, *Nature*, 1991, **353**, 737–740.
- A. Mishra, M. K. R. Fischer and P. Bauerle, *Angew. Chem., Int. Ed.*, 2009, **48**, 2474–2499.
- W. M. Campbell, A. K. Burrell, D. L. Officer and K. W. Jolley, *Coord. Chem. Rev.*, 2004, **248**, 1363–1379.
- C.-W. Lee, H.-P. L. N. M. Reddy, H.-W. Lee, E. W.-G. Diau and C.-Y. Yeh, *Dyes Pigm.*, 2011, **91**, 317–323.
- K. K. Pasunooti, J.-L. Song, H. Chai, P. Amaladass, W.-Q. Deng and X.-W. Liu, *J. Photochem. Photobiol., A*, 2011, **218**, 219–225.
- D. Daphnomili, G. D. Sharma, S. Biswas, K. R. J. Thomas and A. G. Coutsolelos., *J. Photochem. Photobiol., A*, 2013, **253**, 88–96.
- L. Moreira Goncalves, V. de Zea Brumdez, A. Ribeiro and A. Magaltes Mendes, *Energy Environ. Sci.*, 2008, **1**, 655.
- Q. Wang, W. M. Campbell, E. E. Bonfantini, K. W. Jolley, D. L. Officer and P. J. Walsh, *et al.*, *J. Phys. Chem. B*, 2005, **109**, 15397–15409.
- A. Hagfeldt and M. Gratzel, Molecular photovoltaics, *Acc. Chem. Res.*, 2000, **33**, 269–277.
- M. Gratzel, *et al.*, *Inorg. Chem.*, 2005, **44**, 6841–6851.
- N. Robertson, *et al.*, *Angew. Chem., Int. Ed.*, 2006, **45**, 2338–2345.
- L. Giribabu and R. K. Kanaparthi, *Curr. Sci.*, 2013, **104**, 847–855.
- Y. Tachibana, S. A. Haque, I. P. Mercer, J. R. Durrant and D. R. Klug, *J. Phys. Chem. B*, 2000, **104**, 1198–1205.
- M. K. Nazeeruddin, D. F. Angelis, S. Fantacci, A. Selloni, G. Viscardi and P. Liska, *et al.*, *J. Am. Chem. Soc.*, 2005, **127**, 16835–16847.
- P. Wang, C. Klein, J. E. Moser, R. H. Baker, N. L. C. Ha and R. Charvet, *et al.*, *J. Phys. Chem. B*, 2004, **108**, 17553–17559.
- M. Gratzel, *et al.*, *Photochem. Rev.*, 2003, **4**, 145–153.
- N. Xiang, X. Huang, X. Feng, Y. Liu, B. Zhao, L. Deng, P. Shen, J. Fei and S. Tan, *Dyes Pigm.*, 2011, **88**, 75–83.
- W. M. Campbell, K. W. Jolley, P. Wagner, K. Wagner, P. J. Walsh, K. C. Gordon, L. Schmidt-Mende, M. K. Nazeeruddin, Q. Wang, M. Gratzel and D. L. Officer, *J. Phys. Chem. C*, 2007, **111**, 11760–11762.
- Y. Liu, N. Xiang, X. Feng, P. Shen, W. Zhou, C. Weng, B. Zhao and S. T. Tan, *Chem. Commun.*, 2009, 2499–2501.
- M. Tanaka, S. Hayashi, S. Eu, T. Umeyama, Y. Matano and H. Imahori, *Chem. Commun.*, 2007, 2069–2071.
- M. K. Nazeeruddin, R. Humphry-Baker, D. L. Officer, W. M. Campbell, A. K. Burrell and M. Gratzel, *Langmuir*, 2004, **20**, 6514–6517.
- H. Imahori, S. Hayashi, H. Hayashi, A. Oguro, S. Eu, T. Umeyama and Y. Matano, *J. Phys. Chem. C*, 2009, **113**, 18406–18413.
- S. Hayashi, M. Tanaka, H. Hayashi, S. Eu, T. Umeyama, Y. Matano, Y. Araki and H. Imahori, *J. Phys. Chem. C*, 2008, **112**, 15576–15585.
- W. M. Campbell, K. W. Jolley, P. Wagner, K. Wagner, P. J. Walsh, K. C. Gordon, L. Schmidt-Mende, M. K. Nazeeruddin, Q. Wang, M. Gratzel and D. L. Officer, *J. Phys. Chem. C*, 2007, **111**, 11760–11762.
- E. E. Bonfantini, A. K. Burrell, W. M. Campbell, M. J. Crossley, J. J. Gosper, M. M. Harding, D. L. Officer and D. C. W. Reid, *J. Porphyrins Phthalocyanines*, 2002, **6**, 708–719.
- Q. Wang, W. M. Campbell, E. E. Bonfantini, K. W. Jolley, D. L. Officer, P. J. Walsh, K. Gordon, R. Humphrybaker, M. K. Nazeeruddin, M. Gratzel and D. L. Officer, *J. Phys. Chem. B*, 2005, **109**, 15397–15409.

- 27 N. K. Subbaiyan, L. Obraztsov, C. A. Wijesinghe, K. Tran, W. Kutner and F. D'Souza, *J. Phys. Chem. C*, 2009, **113**, 8982–8989.
- 28 N. Kristian, Y. L. Yu, P. Gunawan, R. Xu, W.-Q. Deng, X.-W. Liu and X. Wang, *Electrochim. Acta*, 2009, **54**, 4916–4924.
- 29 C. W. Lee, H. P. Lu, C. M. Lan, Y. L. Huang, Y. R. Liang, W. N. Yen, Y. C. Liu, Y. S. Lin, E. W. G. Diau and C. Y. Yeh, *Chem. – Eur. J.*, 2009, **15**, 1403–1412.
- 30 S. Mathew, A. Yella, P. Gao, R. Humphry-Baker, B. F. E. Curchod, N. Ashari-Astani, I. Tavernelli, U. Rothlisberger, M. K. Nazeeruddin and M. Gratzel., *Nature*, 2014, **6**, 242–247.
- 31 C. Y. Lin, C. F. Lo, L. Luo, H. P. Lu, C. S. Hung and E. W. G. Diau, *J. Phys. Chem. C*, 2009, **113**, 755–764.
- 32 K. D. Seo, M. J. Lee, H. M. Song, H. S. Kang and H. K. Kim, *Dyes Pigm.*, 2012, **94**, 143–149.
- 33 V. V. Pavlishchuk and A. W. Addison, *Inorg. Chim. Acta*, 2000, **298**, 97–102.
- 34 D. P. Hagberg, J.-H. Yum, H. Lee, F. D. Angelis, T. Marinado, K. M. Karlsson, R. Humphry-Baker, L. Sun, A. Hagfeldt, M. Grätzel and M. K. Nazeeruddin, *J. Am. Chem. Soc.*, 2008, **130**, 6259–6266.
- 35 J. K. Park, H. R. Lee, J. Chen, H. Shinokubo, A. Osuka and D. Kim, *J. Phys. Chem. C*, 2008, **112**, 16691–16699.
- 36 A. Luechai, N. Pootrakulchote, T. Kengthanomma, P. Vanalabhpataana and P. Thamyongkit, *J. Organomet. Chem.*, 2014, **753**, 27–33.
- 37 M. J. Frisch, G. W. Trucks, H. B. Schlegel, G. E. Scuseria, M. A. Robb, J. R. Cheeseman, G. Scalmani, V. Barone, B. Mennucci, G. A. Petersson, H. Nakatsuji, M. Caricato, X. Li, H. P. Hratchian, A. F. Izmaylov, J. Bloino, G. Zheng, J. L. Sonnenberg, M. Hada, M. Ehara, K. Toyota, R. Fukuda, J. Hasegawa, M. Ishida, T. Nakajima, Y. Honda, O. Kitao, H. Nakai, T. Vreven, J. A. Montgomery, Jr., J. E. Peralta, F. Ogliaro, M. Bearpark, J. J. Heyd, E. Brothers, K. N. Kudin, V. N. Staroverov, R. Kobayashi, J. Normand, K. Raghavachari, A. Rendell, J. C. Burant, S. S. Iyengar, J. Tomasi, M. Cossi, N. Rega, J. M. Millam, M. Klene, J. E. Knox, J. B. Cross, V. Bakken, C. Adamo, J. Jaramillo, R. Gomperts, R. E. Stratmann, O. Yazyev, A. J. Austin, R. Cammi, C. Pomelli, J. W. Ochterski, R. L. Martin, K. Morokuma, V. G. Zakrzewski, G. A. Voth, P. Salvador, J. J. Dannenberg, S. Dapprich, A. D. Daniels, Ö. Farkas, J. B. Foresman, J. V. Ortiz, J. Cioslowski and D. J. Fox, *Gaussian 09, Revision D.01*, Gaussian, Inc., Wallingford CT, 2009.
- 38 D. Becke, Density-functional thermochemistry. III. The role of exact exchange, *J. Chem. Phys.*, 1993, **98**, 5648–5652.
- 39 A. D. McLean and G. S. Chandler, Contracted Gaussian-basis sets for molecular calculations. 1. 2nd row atoms, $Z = 11-18$, *J. Chem. Phys.*, 1980, **72**, 5639–5648.
- 40 T. Yanai, D. Tew and N. Handy, A new hybrid exchange-correlation functional using the Coulomb-attenuating method (CAM-B3LYP), *Chem. Phys. Lett.*, 2004, **393**, 51–57.